

Comparison of helium bubble formation in F82H, ODS, SIMP and T91 steels irradiated by Fe and He ions simultaneously

Bingsheng Li(李炳生), Zhen Yang(杨振), Shuai Xu(徐帅), Kongfang Wei (魏孔芳), Zhiguang Wang(王志光), Tielong Shen(申铁龙), Tongmin Zhang(张桐民), and Qing Liao(廖庆)

Citation: Chin. Phys. B, 2021, 30 (**3**): 036102. DOI: 10.1088/1674-1056/abc2b4
Journal homepage: http://cpb.iphy.ac.cn; http://iopscience.iop.org/cpb

What follows is a list of articles you may be interested in

Characterization of swift heavy ion tracks in MoS_2 by transmission electron microscopy

Li-Jun Xu(徐丽君), Peng-Fei Zhai(翟鹏飞)†, Sheng-Xia Zhang(张胜霞), Jian Zeng(曾健), Pei-Pei Hu(胡培培), Zong-Zhen Li(李宗臻), Li Liu(刘丽), You-Mei Sun(孙友梅), and Jie Liu(刘杰)‡

Chin. Phys. B, 2020, 29 (**10**): 106103. DOI: 10.1088/1674-1056/abad1e

Comparison of cavities and extended defects formed in helium-implanted 6H-SiC at room temperature and 750 ℃

Qing Liao(廖庆), Bingsheng Li(李炳生), Long Kang(康龙), Xiaogang Li(李小刚)

Chin. Phys. B, 2020, 29 (**7**): 076103. DOI: 10.1088/1674-1056/ab8abc

Defects and electrical properties in Al-implanted 4H-SiC after activation annealing

Yi-Dan Tang(汤益丹), Xin-Yu Liu(刘新宇), Zheng-Dong Zhou(周正东), Yun Bai(白云), Cheng-Zhan Li(李诚瞻)

Chin. Phys. B, 2019, 28 (**10**): 106101. DOI: 10.1088/1674-1056/ab3cc2

Effects of helium irradiation dose and temperature on the damage evolution of Ti_3SiC_2 ceramic

Hua-Hai Shen(申华海), Xia Xiang(向霞), Hai-Bin Zhang(张海斌), Xiao-Song Zhou(周晓松), Hong-Xiang Deng(邓洪祥), Xiao-Tao Zu(祖小涛)

Chin. Phys. B, 2019, 28 (**7**): 076104. DOI: 10.1088/1674-1056/28/7/076104

Scanning transmission electron microscopy: A review of high angle annular dark field and annular bright field imaging and applications in lithium-ion batteries

Yu-Xin Tong(仝毓昕), Qing-Hua Zhang(张庆华), Lin Gu(谷林)

Chin. Phys. B, 2018, 27 (**6**): 066107. DOI: 10.1088/1674-1056/27/6/066107

Comparison of helium bubble formation in F82H, ODS, SIMP and T91 steels irradiated by Fe and He ions simultaneously*

Bingsheng Li(李炳生)[1,†], Zhen Yang(杨振)[2,‡], Shuai Xu(徐帅)[1], Kongfang Wei (魏孔芳)[3], Zhiguang Wang(王志光)[3], Tielong Shen(申铁龙)[3], Tongmin Zhang(张桐民)[3], and Qing Liao(廖庆)[1]

[1] *State Key Laboratory for Environment-Friendly Energy Materials, Southwest University of Science and Technology, Mianyang* 621010, *China*
[2] *Sino-French Institute of Nuclear Engineering and Technology, Sun Yat-sen University, Zhuhai* 519082, *China*
[3] *Institute of Modern Physics, Chinese Academy of Sciences, Lanzhou* 730000, *China*

(Received 21 September 2020; revised manuscript received 19 October 2020; accepted manuscript online 20 October 2020)

Ferritic-martensitic steels and ODS steels are attractive candidates for structural materials in advanced nuclear-power systems due to their good swelling resistance. Four kinds of steels, F82H, 15Cr-ODS, SIMP and T91, are investigated in this study. We take 6.4 MeV Fe^{3+} ions and energy-degraded 1.0 MeV He^{+} ions in the irradiation of these materials to 5 dpa and 60 appm He/dpa, 200 appm He/dpa and 600 appm He/dpa at 300 °C and 450 °C, respectively. The bubble formation and distribution are investigated by transmission electron microscopy (TEM). Formation and distribution of the bubbles in the four investigated steels are compared. The influence of irradiation temperature and helium injection ratio on bubble formation is discussed. It is found that there appears to be homogenously distributed bubbles at 300 °C irradiation while heterogeneously distributed bubbles at 450 °C irradiation.

Keywords: martensitic steels, Fe and He co-irradiation, He bubbles, transmission electron microscopy

PACS: 61.80.–x, 61.80.Jh, 68.37.Lp, 78.40.Kc **DOI:** 10.1088/1674-1056/abc2b4

1. Introduction

The greenhouse effect is caused by the excessive carbon dioxide in air. It is generally accepted that the greenhouse effect is resulted from industrial activities, and it has a severe effect on the natural environment and ecosystems. It is therefore very important to decrease the total amount of carbon dioxide produced by the rapidly developing modern society. It is well known that nuclear energy is regarded as a kind of clean energy with nearly zero carbon emission. In China, fission nuclear power is rapidly developing and far more new nuclear power plants will be built in future. Chernobyl and Fukushima nuclear accidents have called for new concepts of nuclear reactors with a high level of inherent safety. In order to avoid nuclear accidents and to use fuel more efficiently through higher levels of burn-up, many new concepts of nuclear-energy systems have been developed recently, such as AP1000, HPR 1000, TMSR, ADS, fast reactor, high-temperature gas-cooled reactor. In advanced nuclear power systems, the structural materials suffered from more serious problems, such as strong particle irradiation, high operation temperature, corrosion, loading stress. As a result, much more pronounced degradation processes, such as the ductile-to-brittle transition shift, creep, swelling, fatigue, cause a severe degradation of material properties.[1–4] Some new materials are needed to satisfy the demand of advanced nuclear reactors.

Due to their good swelling resistance under neutron irradiation, high thermal conductivity and low thermal expansion coefficient, iron-chromium-based alloys including ferritic-martensitic (FM) steels and oxide dispersion strengthened (ODS) alloys are considered as some of the main candidate structural materials for advanced nuclear reactors.[5,6] T91 and F82H steels, which belong to two primary FM steels, have been extensively investigated by irradiation, including neutron, ions and electron. SIMP steel, new developed FM steel for the special environment of ADS, was designed and fabricated by the Institute of Modern Physics and Institute of Metal Research, Chinese Academy of Sciences.[7] Due to some shortcomings of neutron irradiated new developed structural materials, such as high cost, strong radioactivity and low irradiation dose (typical damage rate of displacements per toms per second (dpa/s) is on the order of 10^{-8}–10^{-6} dpa/s). Therefore, using ion irradiation ($\sim 10^{-5}$–10^{-3} dpa/s) emulates neutron damage is a faster and efficient method. Many reports of ions successfully replicated the features of the microstructure in neutron irradiated structural materials.[8–10]

In advanced nuclear reactor surroundings, structural materials suffered from intense neutron irradiation. A great amount of He atoms are formed by the (n, α) nuclear reaction. Due to a very low solubility in FM alloys, He atoms easily migrate and accumulate in irradiation-induced vacancy

*Project supported by the National Natural Science Foundation of China (Grant Nos. U1832133 and 12075194), the Sichuan Science and Technology Program, China (Grant No. 2020ZYD055), and the Doctor Research Foundation of Southwest University of Science and Technology (Grant No. 18zx714101).

†Corresponding author. E-mail: libingshengmvp@163.com
‡Corresponding author. E-mail: yangzh97@mail.sysu.edu.cn

© 2021 Chinese Physical Society and IOP Publishing Ltd

clusters to form nano-scaled bubbles.[11–14] It has been reported that bubbles are easily formed on grain boundaries at 400 °C and above, resulting in grain boundary helium embrittlement in the long-term survival of materials in nuclear power systems.[15] Below 400 °C, cavities are homogeneously distributed in grains, resulting in grain swelling and hardness.[16] Therefore, it is important to investigate the formation of cavities in FM alloys. Because neutron irradiation is often accompanied by generation of He atoms, it is necessary to use dual- or triple-beam accelerators that provide heavy ions and He ions simultaneously. It has been reported that He generation rate ranges 0.1–100 appm He/dpa (dpa: displacements per atom) based on different nuclear reactors. Due to the main component of FM steels is iron, Fe irradiation does not introduce impurities. He atoms are provided by He^+ implantation. Up to now, irradiation hardening via dual or triple beams irradiation into FM steels has been investigated. For example, Lee *et al.*[17] investigated irradiation hardening in 9Cr-2WVTa steel via triple-beam irradiation (H, He and Fe) at 80 °C, 200 °C and 350 °C to 50 dpa with He concentration of 200 appm He/dpa and H concentration of 1000 appm H/dpa, and argued the increase in irradiation hardening in the He and Fe co-irradiated sample compared to only Fe irradiation at 200 °C. Similarly, Ando *et al.*[18] also investigated irradiation hardening in Fe and He co-irradiated F82H steel at 360 °C to 33 dpa with 10 and 100 appm He/dpa, and found more significant irradiation hardening in the dual-beam irradiation. Takayama *et al.*[19] investigated irradiation hardening of F82H steel via Fe and He co-implantation at 290 °C to 3 dpa and 100 appm He/dpa, and argued no significant influence of implanted He atoms on the irradiation hardening. We recently reported irradiation hardening caused by Fe and He co-irradiated F82H, 15Cr-ODS, SIMP and T91 steels at 300 °C and 450 °C to 5 dpa and three different He concentrations (60 appm He/dpa, 200 appm He/dpa and 600 appm He/dpa), and found the effect of He concentration and temperature on irradiation hardening.[20] It is important to note that He/dpa ratios between 80 and 100 are typical for spallation neutron target and numerous FM alloys including ODS steels, exposed to such radiation environment, have been microstructurally characterized by TEM and some advanced characterization methods in the past.[21–23] Nonetheless, the fixed He/dpa of the spallation target does not enable to study the effect of this parameter, contrary to ion bombardment experiments.

Besides irradiation hardening, irradiation swelling is also worth investigating. Irradiation swelling induced by neutron or single beam ions has been widely investigated. Garner *et al.*[24] investigated synergistic influence of displacement rate and helium/dpa ratio on swelling of Fe-(9-12)Cr binary alloys in FFTF at 400 °C, and found the increase in swelling rate with increasing dpa rate. The swelling rate ranges from 0.05%/dpa to 0.2%/dpa, which depends on the He generation rate (appm He/dpa). Taller *et al.*[25] investigated bubble and void nucleation in Fe and He co-irradiated T91 at 520 and 570 °C. They argued that bubble stability is related to irradiation temperature (445–570 °C) and helium co-injection rate (0–4 appm He/dpa). Li *et al.*[26] investigated cavity swelling induced by He or Kr irradiated SIMP and T91 steels at different temperatures, and found good swelling resistance of SIMP steel. Wang *et al.*[27] investigated irradiation swelling in a reduced-activation ferritic-martensitic steel irradiated by Fe ions with 10 appm and 100 appm pre-implanted He at 460 °C, and found the increase in C and Cr concentrations in FM steels to precipitate $(Fe, Cr)_2C$ during radiation to improve swelling resistance. We recently investigated the cavity growth in Fe-11 wt.%Cr alloy under *in situ* observation during high-voltage electron irradiation, and found that the mean size of cavities decreased when He atoms were pre-implanted.[28] However, to date, a comprehensive study of the bubble formation in FM steel irradiated by Fe and He simultaneously is missing. Using single beam ion irradiation cannot really simulate the effect of neutron irradiation, although it enables to study a wide range of He/dpa ratio, when using a depth sensitive characterization technique.[12] Therefore, the aim of this study is to investigate the bubble formation in four kinds of structural materials via Fe and He co-irradiation at 300 °C and 450 °C with three different He concentrations (60 appm He/dpa, 200 appm He/dpa and 600 appm He/dpa) by transmission electron microscopy (TEM). The research results will be useful to elucidate the effect of He concentration on swelling in nuclear structural steels.

2. Experimental process

Table 1 presents the nominal composition of the present experimental F82H, T91, SIMP and 15Cr-ODS steels. The thermal treatment procedure is: F82H was normalized at 1040 °C for 30 min and tempered at 740 °C for 60 min. T91 was normalized at 1040 °C for 60 min and tempered at 760 °C for 60 min. SIMP was normalized at 1050 °C for 30 min and tempered at 760 °C for 90 min. ODS (Fe-15Cr) ferritic steel was normalized at 1150 °C and tempered at 1150 °C for 60 min. All the specimens were cut into 5 mm ×2 mm ×1 mm in size. Surfaces of the samples were mechanically polished with sandpapers (600–4000 grades), and then to fine mirror finish with 0.1 μm diamond spray. Finally, the specimens were electrochemical polishing at room temperature with 25 V and 20 s in a 5 vol.% perchloric acid and 95 vol.% methanol solution.

Dual-beam irradiation experiments were carried out at DuET in Kyoto University. There were 6.4 MeV Fe^{3+} ions provided by a 1.7 MeV tandem accelerator with a simultaneous implantation of energy-degraded 1.0 MeV He^+ ions

(through three different thicknesses of Al films) from a 1.0 MV Singletron accelerator. In order to supply uniform ion fluence, the beams were raster scanned. The irradiation temperatures were well controlled at 300±5 °C and 450 °C±5 °C and the irradiation temperature was measured by an infrared thermometer. Using the Monte–Carlo code Stopping and Range of Ions in Matter (SRIM-2008) quick cascade simulations to calculate depth profiles of the Fe irradiation-induced displacement damage and the implanted helium (the threshold displacement energy of 40 eV and the density of 7.86 g/cm^3),[29] as shown in Fig. 1. The nominal displacement damage rate, nominal displacement damage were 3×10^{-4} dpa/s and 5 dpa at a depth of 600 nm, respectively. In order to investigate the influence of He concentration on bubble formation, we took three different helium injection ratios of 60 appm He/dpa, 200 appm He/dpa and 600 appm He/dpa.

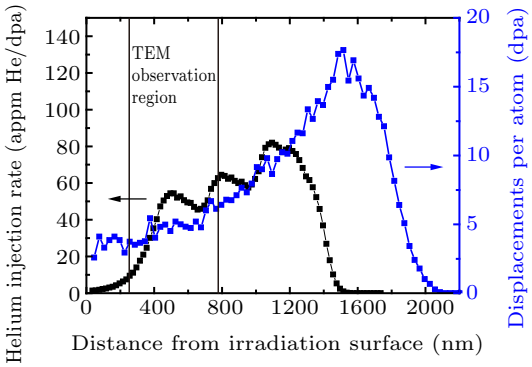


Fig. 1. Depth profiles of the displacement damage induced by 6.4 MeV Fe irradiation to a fluence of 1.65×10^{16} ions/cm^2 and the helium deposition via 1.0 MeV He irradiation through an energy-degraded facility.

JEOL 2010 TEM operating at 200 keV was used to observe bubble distribution at depth ranging from approximately 350 nm to 700 nm. Cross-sectional TEM specimens were fabricated by a Hitachi 2000 focused ion beam (FIB) system. The irradiated surface was protected via deposited a tungsten film with 1–2 μm thickness. The fabrication process of XTEM was described in our previous article.[20] The thickness of observed zone was measured by convergent beam electron diffraction (CBED) method. The size and number density of the observed cavities were measured by Nano Measurer software.

3. Results and discussion

Figure 2 shows an over-viewed image of bubble distribution in Fe and He co-irradiated F82H to 600 appm He/dpa at 450 °C. Cavities exhibit bright spots with a round geometry under the under-focused condition. It can be seen that cavities are observed from the near sample surface to a depth of 1280 nm, which is consistent with the helium deposition simulated by SRIM-2008. Cavities are observed in grain interiors, along dislocations, on lath boundaries and at precipitate-matrix interfaces. Bubbles are almost homogeneously distributed with depth due to the uniform helium concentration in this region. Therefore, in this article, the cavity formation and distribution in the depth ranging from about 200 to 500 nm were investigated.

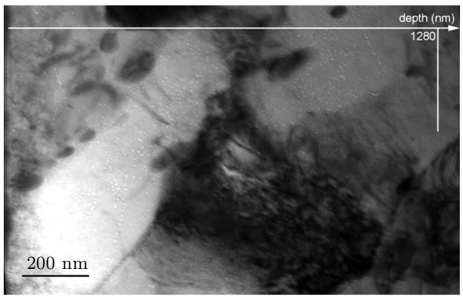


Fig. 2. The bubble distribution in the Fe and He co-irradiated F82H steel characterized by XTEM. The XTEM bright-field image shows bubble distribution with depth in Fe and He co-irradiated F82H to 600 appm He/dpa at 450 °C. Cavities are observed from the sample surface to a depth of about 1280 nm under the under-focused condition with $\Delta f=-512$ nm. The sample surface is located on left.

Figure 3 shows the bubble formation in the near surface region of Fe and He co-irradiation at 300 °C. Bubbles are scattered distributed in four steels when He injection ratio is 60 appm He/dpa. The number of observed cavities increases with the increasing He injection ratio. At 600 appm He/dpa, a high density of nano-sized bubbles is homogeneously distributed in grain interiors. The size and distribution of observed bubbles are similar among these steels. It is demonstrated that the influence of oxide particles on bubble nucleation decreases with the increasing helium concentration. The size distribution and number density of observed bubbles are analyzed, as shown in Fig. 4.

Figure 4 shows the bubble size distribution in these four steels after Fe and He co-irradiation at 300 °C. It shows a skewed distribution in these figures. At 60 appm He/dpa, the size of observed bubbles is the largest in SIMP, next to T91. It is the smallest in 15Cr-ODS. Increasing helium injection ratio, the average size of observed bubbles decreases, while the number density significantly increases from 10^{22} m^{-3} to 10^{23} m^{-3}. At 600 appm He/dpa, the diameter of observed bubbles in the F82H, 15Cr-ODS and T91 is in the range of 1 to 4 nm. Only a few large bubbles with a diameter of about 7 nm are observed in the SIMP. It can be seen that the average size of observed bubbles does not have a significant change with increasing helium injection ratio in the 15Cr-ODS, unlike in the SIMP and T91. It can be accounted for oxide particles, acting as sinks for radiation-induced defects and/or helium and can control bubble nucleation and growth. The average size of observed bubbles decreases with increasing helium concentration. It is demonstrated that helium atoms can restrict vacancy diffusion, and nano-scaled bubbles were homogeneously formed in the helium deposition region. This result is consistent with other reports.[16,30]

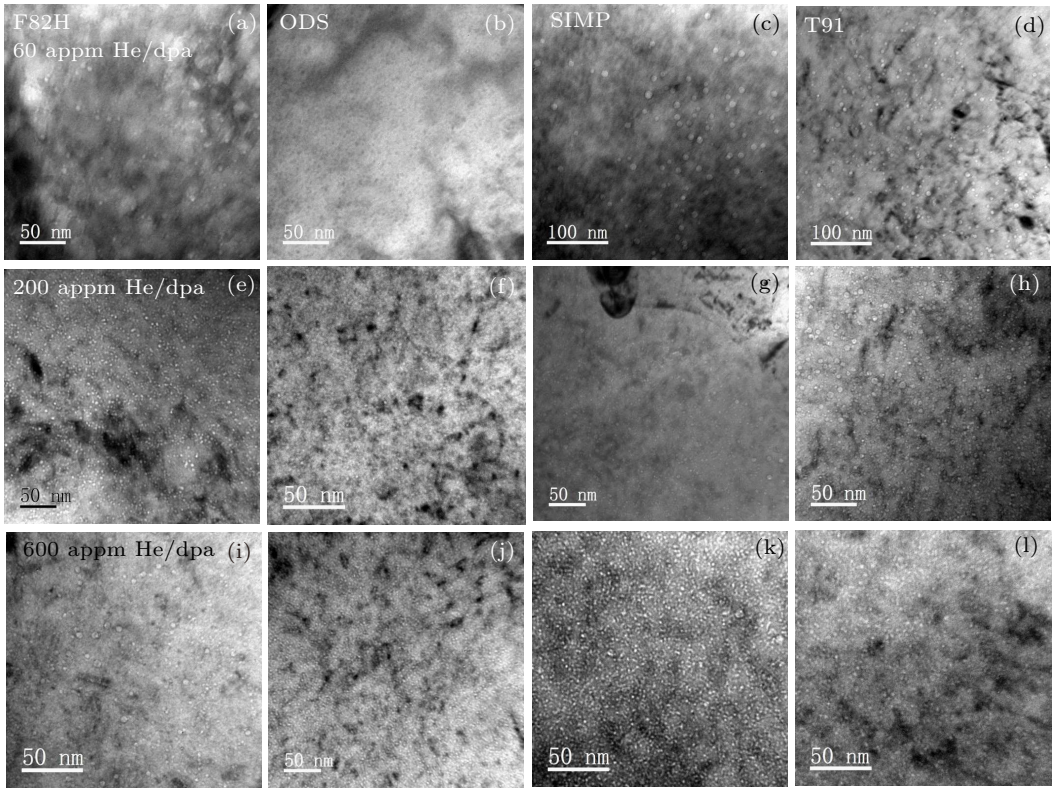


Fig. 3. XTEM bright-field images under the under-focused condition showing bubble formation in the Fe and He co-irradiated F82H (a, e, i), 15Cr-ODS (b, f, j), SIMP (c, g, k) and T91 (d, h l) to 60 appm He/dpa (a, b, c, d), 200 appm He/dpa (e, f, g, h) and 600 appm He/dpa (i, j, k, l), respectively. The experiment was performed at 300 °C. Note that the 15Cr-ODS shown in (b) was observed under the over-focused condition that bubbles present dark fringes.

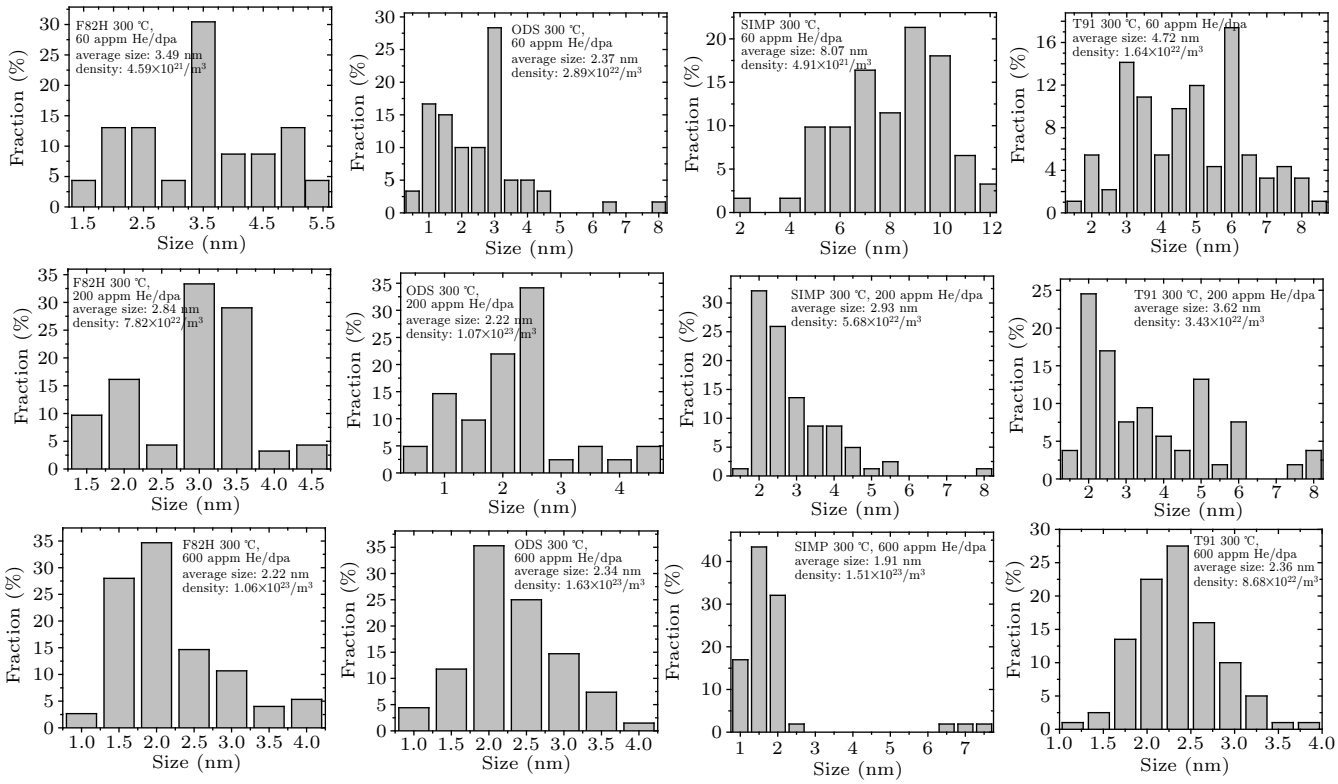


Fig. 4. Size distribution of observed bubbles in the Fe and He co-irradiated F82H, 15Cr-ODS, SIMP and T91 with different He injection ratios at 300 °C.

Figure 5 shows the cavity formation in the near surface region of Fe and He co-irradiation into four kinds of steels at 450 °C. Nano-scaled bubbles exhibit bright dots under the under-focused condition. For F82H, SIMP and T91, some bubbles appeared as pearl-like distribution, where dislocations were observed by two-beam bright-field condition.

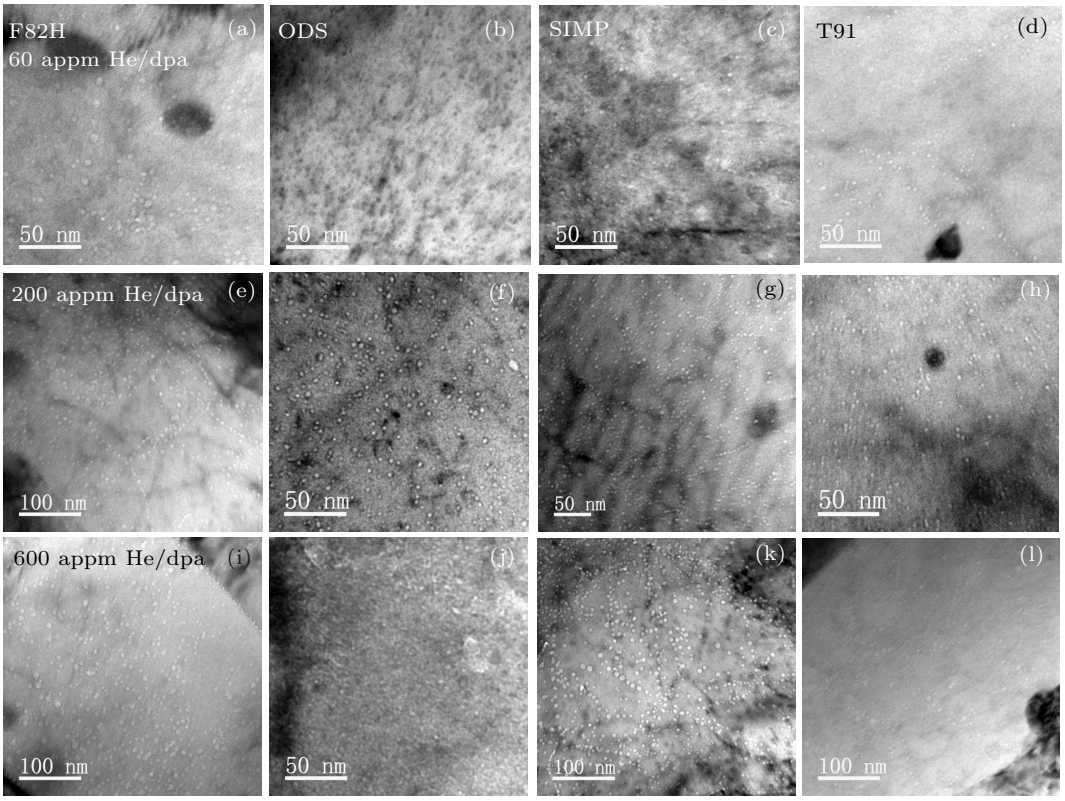


Fig. 5. XTEM bright-field images under under-focused condition showing bubble formation in the Fe and He co-irradiated F82H (a, e, i), 15Cr-ODS (b, f, j), SIMP (c, g, k) and T91 (d, h l) to 60 appm He/dpa (a, b, c, d), 200 appm He/dpa (e, f, g, h) and 600 appm He/dpa (i, j, k, l), respectively. Note that (a, b, c) have the same scale as (d); while (e, f, g) have the same scale as (h); and (i, k) have the same scale as (l). The experiment was performed at 450 °C. Note that (b) was imaged under the over-focused condition with $\Delta f = 304$ nm.

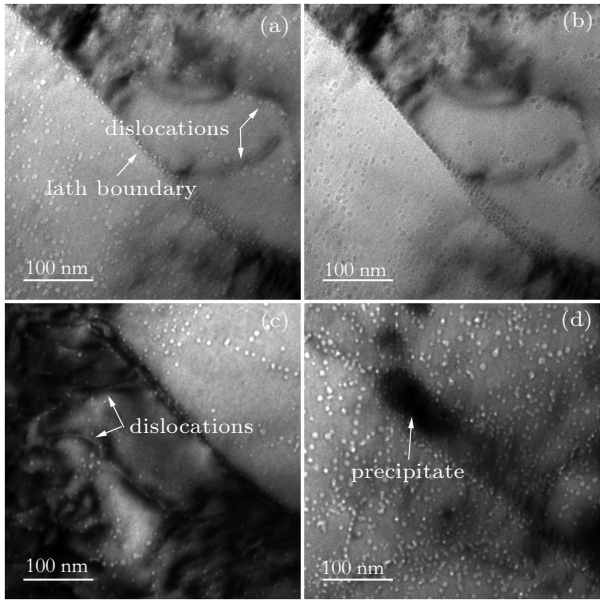


Fig. 6. XTEM images of bubble formation of the Fe and He co-irradiated F82H to 600 appm He/dpa at 450 °C, bubbles at lath boundaries viewed by the under-focused condition (a) and the over-focused condition (b), along dislocations (c) and at a carbide precipitate-matrix interface (d).

In addition, bubbles are easily observed at both grain boundaries and lath boundaries and precipitate-matrix interfaces, such as a high density of bubbles lying along two lath boundaries shown in Fig. 6. This result indicates that bubbles are preferential to nucleate along dislocations, at precipitate-matrix interfaces and lath boundaries at 450 °C, but not at 300 °C. It is attributed to the fact that small helium-vacancy clusters are no longer thermally stable and thus some helium atoms diffuse inside the material. These helium atoms at 450 °C diffused easily to reach microstructural sinks, such as dislocations, grain boundaries. The sink strength for helium atoms depends on helium-defect binding energy. The large binding energy indicates the strong sink strength. First principle calculations have demonstrated the binding energy of He atoms with vacancies that ranges from 0.78 eV to 3.16 eV.[31] Vacancies can be produced by irradiation and mechanical alloying, such as grain boundaries and precipitate-matrix interface.[15] In addition, the binding energies of helium atoms with an edge dislocation, such as 2.3 eV for a perfect dislocation loops and 1.0 eV for a screw dislocation line.[32,33] When vacancies trap helium atoms to form vacancy-helium clusters, the vacancies would drag He atoms to grain boundaries, lath boundaries, precipitate-matrix interfaces and dislocations based on migration and coalescence mechanism.

Figure 7 shows bubble distribution in the Fe and He co-irradiated 15Cr-ODS to 200 appm He/dpa at 450 °C. Helium bubbles were formed at the surface of oxide particles. Fewer bubbles were observed on grain boundaries. It is usually seen that the cohesion intensity of grain boundaries decreases significantly when dense helium bubbles formed on grain bound-

aries, resulting in occurrence of helium embrittlement during deformation. Oxide particles have a large surface area that can efficiently trap vacancy-helium clusters, in order to reduce the number of vacancy-helium clusters on grain boundaries. Therefore, a high-number density of bubbles was found at the surface of oxide particles. This result demonstrates that 15Cr-ODS steel has a good ability of resistant helium embrittlement at elevated operational temperatures. It has been reported that 15Cr-ODS steel is regarded as the main candidate material used in future fusion reactors and advanced fission systems.[34]

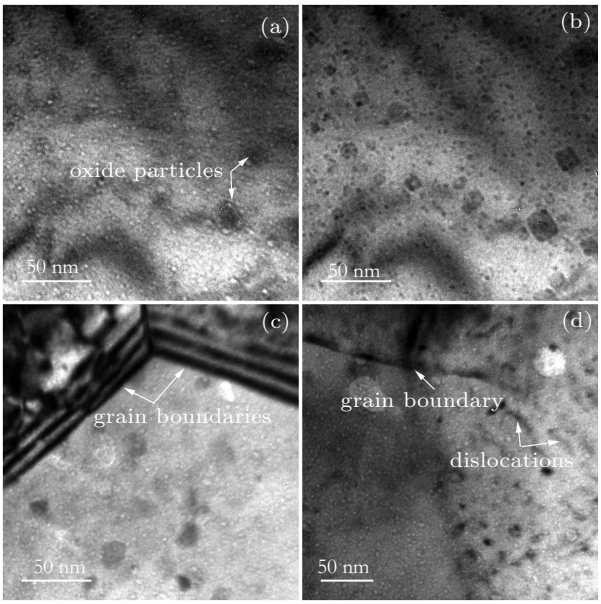


Fig. 7. XTEM images of bubble formation of the Fe and He co-irradiated 15Cr-ODS to 200 appm He/dpa at 450 °C, bubbles formed on the surface of oxide particles viewed by the under-focused condition (a) and the over-focused condition (b), on grain boundaries and dislocations (c, d). Oxide particles exhibit hexahedron and sphere shape with dark contrasts.

The size and number density of the observed bubbles shown in Fig. 5 were analyzed, as shown in Fig. 8. Similar to the case of 300 °C irradiation, it also shows a skewed distribution in these figures. The average size of observed bubbles increases with increasing helium injection ratio, except for 15Cr-ODS. This trend is contrary to the case of 300 °C irradiation. According to the critical bubble model concept, the bubble growth rate can be expressed as[35]

$$\frac{\mathrm{d}r}{\mathrm{d}t} = \frac{\Omega}{r}\left[D_{\mathrm{v}}C_{\mathrm{v}} - D_{\mathrm{i}}C_{\mathrm{i}} - D_{\mathrm{v}}C_{\mathrm{v}}\exp\left(\frac{2\gamma}{r} - p_{\mathrm{g}}\right)\right], \quad (1)$$

where D_{v} and D_{i} are vacancy and interstitial diffusion coefficient, respectively, C_{v} and C_{i} are vacancy and interstitial concentration, Ω is the atomic volume, γ is the surface energy, and p_{g} is the inner pressure of bubbles, which is given by $p = 3\kappa mkT/4\pi r^3$, with κ being the real gas compressibility factor. The growth of the bubble depends on the arrival of vacancies to the bubble. On the contrary, the reduction in bubble radius r depends on the arrival of interstitial to the bubble. Bubbles also emit vacancies under high temperature, resulting in shrinkage at a rate given by the capillary approximation as

$$\frac{\mathrm{d}r}{\mathrm{d}t} = D_{\mathrm{v}}C_{\mathrm{v}}\exp\left(\frac{2\gamma}{r} - p_{\mathrm{g}}\right). \quad (2)$$

Growth stability and instability conditions depend on the $\mathrm{d}r/\mathrm{d}t = 0$, when

$$D_{\mathrm{v}}C_{\mathrm{v}} - D_{\mathrm{i}}C_{\mathrm{i}} - D_{\mathrm{v}}C_{\mathrm{v}}\exp\left(\frac{2\gamma}{r} - p_{\mathrm{g}}\right) = 0. \quad (3)$$

The change in defect concentration of interstitials and vacancies with time can be expressed as

$$\frac{\mathrm{d}C_{(i,v)}}{\mathrm{d}t} = K_0 - K_{\mathrm{iv}}C_{\mathrm{i}}\left(C_{\mathrm{v}} + C_{\mathrm{v,T}}\right) - k^2_{(\mathrm{i,v})}D_{(\mathrm{i,v})}C_{(\mathrm{i,v})}, \quad (4)$$

where $k^2_{(\mathrm{i,v})}$ is the sink strength for interstitials or vacancies, respectively. K_0 is the production rate of defects, and $K_{\mathrm{iv}}C_{\mathrm{i}}\left(C_{\mathrm{v}} + C_{\mathrm{v,T}}\right)$ is the annihilation of the point defects due to thermal recovery. The growth of bubbles increases with increasing D_{v} and p_{g}. Because the migration energies of vacancies and interstitials are 0.62 eV and 0.35 eV,[36] respectively, vacancies and interstitials can rapidly diffuse at 450 °C, resulting in the increasing value of $K_{\mathrm{iv}}C_{\mathrm{i}}\left(C_{\mathrm{v}} + C_{\mathrm{v,T}}\right)$. Thus, the concentrations of residual interstitials and vacancies are available for defect nucleation decrease. However, vacancies can efficiently trap helium atoms to form vacancy-helium clusters, which can stabilize vacancies, in order to avoid vacancy-interstitial recombination. With increasing helium injection ratio, more helium atoms are introduced in the damaged region. These helium atoms can stabilize Fe irradiation-induced vacancies, and therefore more vacancies are available to participate in bubble nucleation. In addition, the gas pressure increases with increasing helium atoms. Increasing helium gas pressure can enhance the growth of bubbles. The rapid growth of vacancy-helium clusters at 450 °C induces the increase in average size of bubbles with increasing helium injection ratio. On the contrary, the growth rate of vacancy-helium clusters is slow at 300 °C. Increasing helium injection ratio, it can form more vacancy-helium clusters. These vacancy-helium clusters grew slowly at 300 °C, resulting in a high number density of bubbles with 2–3 nm diameter. In comparison with 300 °C irradiation, the number density decreases, while the average size increases after 450 °C irradiation. It can be attributed to increasing dynamic annealing at 450 °C. Our recent article[20] reported that the irradiation hardening is almost negligible at 450 °C irradiation, while it increases almost 100% at 300 °C irradiation. It is interesting to note why the average size of observed bubbles in the Fe and He co-irradiated SIMP and T91 to 60 appm He/dpa at 300 °C is larger than Fe and He co-irradiation to the same helium injection ratio at 450 °C. It may be attributed to the influence of dislocation

loops. At 300 °C irradiation, most of the dislocation loops belong to interstitial type.[37] There is a high density of dislocation loops formed after Fe and He co-irradiation. Irradiation-induced interstitials participate in forming dislocation loops, meanwhile irradiation-induced vacancies participate in bubble nucleation. Dislocation loops can sink for helium atoms, resulting in the increase in helium gas pressure that can accelerate bubble growth. Therefore, large bubbles are found in Figs. 3(c) and 3(d). In these four kinds of steels, only 15Cr-ODS has an insignificant change of the size distribution with irradiation temperature and helium injection ratio. Oxide particles can explain this phenomenon that vacancy diffusion can be retarded by oxide particles, resulting in a lower swelling rate after neutron irradiation compared to ferritic-martensitic steels.[38–41]

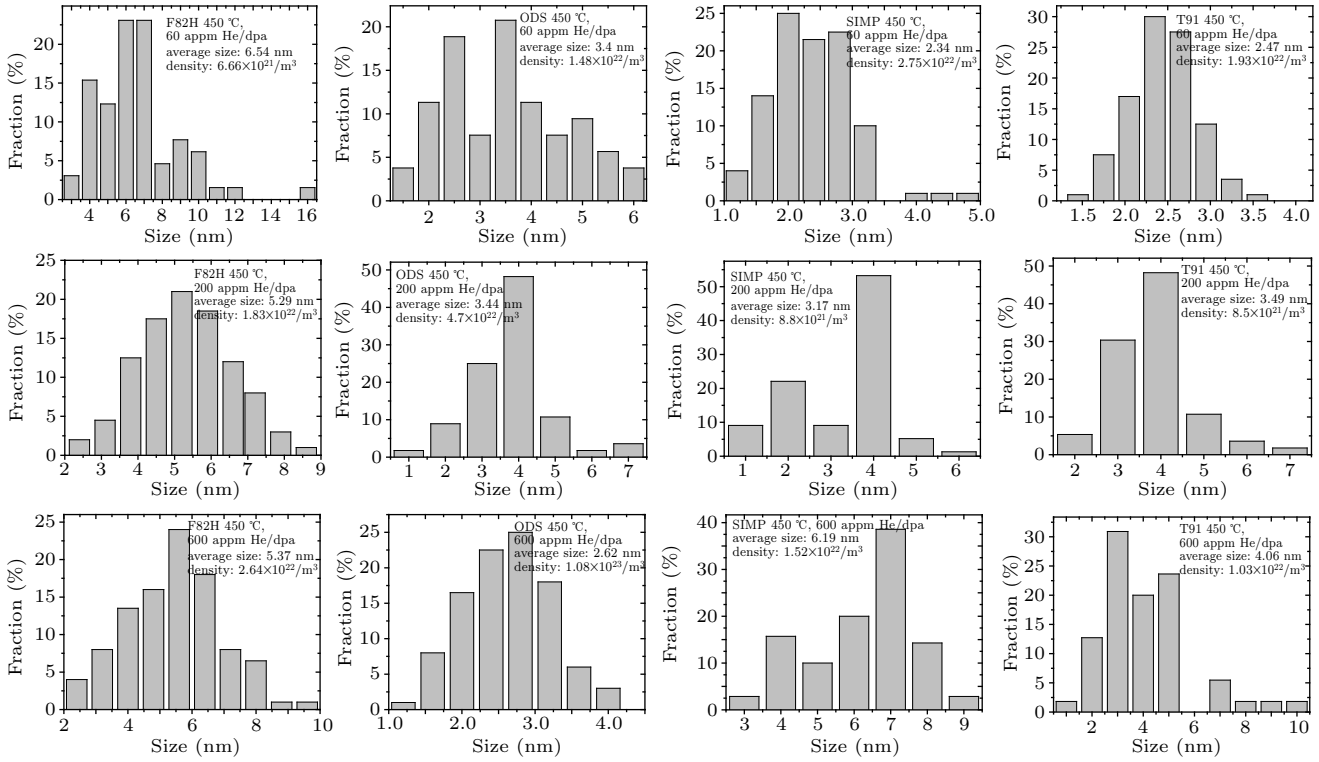


Fig. 8. Size distribution of observed bubbles in the Fe and He co-irradiated F82H, 15Cr-ODS, SIMP and T91 with different He injection ratios at 450 °C.

4. Conclusions

We have investigated the formation of He bubbles in the Fe and He co-irradiated F82H, 15Cr-ODS, SIMP and T91 at 300 °C and 450 °C. In order to investigate the influence of the helium injection ratio on bubble formation, three different helium injection ratios, 60 appm He/dpa, 200 appm He/dpa and 600 appm He/dpa, were carried out. It is determined that irradiation temperature and helium injection ratio significantly influence the size distribution and number density of bubbles. The average size of bubbles increases, while their number density decreases with increasing irradiation temperature. At 300 °C irradiation, bubbles are homogenously distributed. The average size of bubbles decreases with increasing helium injection ratio. It is contrary to the case of 450 °C irradiation. Bubbles are heterogeneously distributed in the Fe and He co-irradiated F82H, SIMP and T91 at 450 °C, such as the preferential bubble nucleation on grain boundaries, precipitates and dislocations due to the strong sink strength of helium atoms at these sites. Few bubbles are observed on grain boundaries of the Fe and He co-irradiated ODS at 450 °C. There are numerous oxide particles that can retard vacancy migration in ODS, and thus the changes of bubble size and bubble density are less significant than other three FM steels. In comparison with F82H, SIMP and T91, 15Cr-ODS has a better swelling resistance.

References

[1] Garner F A, Toloczko M B and Sencer B H 2000 *J. Nucl. Mater.* **276** 123
[2] Toloczko M B, Garner F A and Maloy S A 2012 *J. Nucl. Mater.* **428** 170
[3] Wakai E, Okubo N, Ando M, Yamamoto T and Takada F 2010 *J. Nucl. Mater.* **398** 64
[4] Hu W H, Guo L P, Chen J H, Luo F F, Li T C, Ren Y Y, Suo J P and Yang F 2014 *Fusion Engin. Design* **89** 324
[5] Zinkle S J and Busby J T 2009 *Mater. Today* **12** 12
[6] Was G S, Petti D, Ukai S and Zinkle S J 2019 *J. Nucl. Mater.* **527** 151837
[7] Peng J, Shen T L, Cui M H, Zhu Y B, Li B S, Zhang T M, Li J Y, Jin S X, Lu E Y, Cao X Z and Wang Z G 2019 *J. Nucl. Mater.* **520** 131
[8] Was G S 2015 *J. Mater. Res.* **30** 1158
[9] Was G S, Jiao Z, Getto E, Sun K, Monterrosa A M, Maloy S A, Anderoglu O, Sencer B H and Hackett M 2014 *Scripta Mater.* **88** 33

[10] Zinkle S J, Snead L L 2018 *Scripta Mater.* **143** 154
[11] Krsjak V, Kuriplach J Shen T, Sabelova V, Sato K and Dai Y 2015 *J. Nucl. Mater.* **456** 382
[12] Krsjak V, Degmova J, Sojak S and Slugen V 2018 *J. Nucl. Mater.* **499** 38
[13] Liu W B, Zhang J H, Ji Y Z, Xia L D, Liu H P, He C H, Zhang C and Yang Z G 2018 *J. Nucl. Mater.* **500** 213
[14] Li B S, Krsjak V, Degmova J, Wang Z G, Shen T L, Liu H, Sojak S, Slugen V and Kawasuso A 2020 *J. Nucl. Mater.* **535** 152180
[15] Edmondson P D, Parish C M, Zhang Y, Hallen A and Miller M K 2013 *J. Nucl. Mater.* **434** 210
[16] Xia L D, Liu W B, Liu H P, Zhang J H, Chen H, Yang Z G and Zhang C 2018 *Nucl. Eng. and Tech.* **80** 132
[17] Lee E H, Hunn J D, Rao G R, Klueh R L and Mansur L K 1999 *J. Nucl. Mater.* **271–272** 385
[18] Ando M, Tanigawa H, Jitsukawa S, Sawai T, Katoh Y, Kohyma A, Nakamura K and Takeuchi H 2002 *J. Nucl. Mater.* **307–311** 260
[19] Takayama Y, Kasada R, Sakamoto Y, Yabuuchi K, Kimura A, Ando M, Hamaguchi D and Tanigawa H 2013 *J. Nucl. Mater.* **442** S23
[20] Li B S, Wang Z G, Wei K F, Shen T L, Yao C F, Zhang H P, Sheng Y B, Lu X R, Xiong A L and Han W T 2019 *Fusion Engin. Design* **142** 6
[21] Krsjak V, Kuriplach J, Cieh C, Peng L and Dai Y 2018 *J. Nucl. Mater.* **504** 277
[22] Krsjak V and Dai Y 2015 *J. Nucl. Mater.* **465** 311
[23] Dai Y, Krsjak V, Kuksenko V and Schaubin R 2018 *J. Nucl. Mater.* **511** 508
[24] Garner F A, Gelles D S, Greenwood L R, Okita T, Sekimura N and Wolfer W G 2004 *J. Nucl. Mater*. **329–333** 1008
[25] Taller S and Was G S 2020 *Acta Mater.* **198** 47
[26] Li Y F, Shen T L and Gao X 2013 *Chin. Phys. Lett.* **30** 126101
[27] Wang J, Gao X and Wang Z G 2015 *Chin. Phys. Lett.* **32** 076101
[28] Li B S, Wang Z G, Shen T L, Wei K F, Sheng Y B, Shibayama T, Lu X R and Xiong A L 2019 *Chin. Phys. Lett.* **36** 046104
[29] http://www.srim.org
[30] Chen J, Jung P, Hoffelner W and Ullmaier H 2008 *Acta Mater.* **56** 250
[31] Fu C C and Willaime F 2005 *Phys. Rev. B* **72** 1
[32] Heinisch H L, Gao F and Kurtz R J 2006 *J. Nucl. Mater.* **351** 141
[33] Heinisch H L, Gao F and Kurtz R J 2007 *J. Nucl. Mater.* **367–370** 311
[34] Parish C M, Unocic K A, Tan L, Zinkle S J, Kond S, Snead L L, Hoelzer D T and Katoh Y 2017 *J. Nucl. Mater.* **483** 21
[35] Was G S 2017 *Fundamentals of Radiation Materials Science* (New York: Springer)
[36] Wharry J P and Was G S 2014 *Acta Mater.* **65** 42
[37] Yao Z, Mayoral M H, Jenkins M L and Kirk M A 2008 *Philos. Mag.* **88** 2851
[38] Castro V de, Marquis E A, Perez S L, Pareja R and Jenkins M L 2011 *Acta Mater.* **59** 3927
[39] Lu C Y, Lu Z, Wang X, Xie R, Li Z Y, Higgins M, Liu C M, Gao F and Wang L M 2017 *Sci. Rep.* **7** 40343
[40] Lu C Y, Lu Z, Xie R, Liu C and Wang L M 2014 *J. Nucl. Mater.* **455** 366
[41] Zhang C H, Yang Y T, Song Y, Chen J, Zhang L Q, Jang J and Kimura A 2014 *J. Nucl. Mater.* **455** 61